Enhanced DOA Estimation Exploiting Multi-Frequency Sparse Array

Shuimei Zhang, *Member, IEEE*, Ammar Ahmed, *Student Member, IEEE*, Yimin D. Zhang, *Fellow, IEEE*, and Shunqiao Sun, *Senior Member, IEEE*

***Abstract*—In this paper, we develop a general framework of multi-frequency sparse array to estimate the direction-of-arrival (DOA) of a significantly higher number of targets than the number of physical sensors. The multi-frequency sparse arrays are designed to offer zero lag redundancy in the rendered difference coarray so that the available degrees of freedom are fully utilized to enable high-resolution DOA estimation. A modified sensor interpolation technique is developed to accurately estimate the signal correlation matrix so that the effect of holes in the difference coarray is mitigated. The proposed technique accounts for both self-lags between signals corresponding to the same frequencies and the cross-lags between signals corresponding to different frequencies. As such, it enhances the DOA estimation performance compared to existing methods that either perform array interpolation utilizing only the self-lags or carry out group sparse reconstruction without exploiting array interpolation. Simulation results verify the offerings of the multi-frequency sparse arrays.**

***Index Terms*—Array interpolation, direction-of-arrival estimation, multi-frequency sparse array, zero lag redundancy, group sparsity.**

I. Introduction

ONE of the fundamental research problems in array signal processing is direction-of-arrival (DOA) estimation, which determines the spatial spectrum of the impinging electromagnetic waves. DOA estimation finds broad applications in radar, radio astronomy, navigation, sonar, wireless communications, and seismology [3], [4]. Traditionally, uniform linear arrays (ULAs) are commonly adopted as a result of the Nyquist sampling theorem. An N-element ULA resolves up to $N-1$ sources or targets, and subspace-based DOA estimation methods, such as MUltiple SIgnal Classification (MUSIC) [5] and Estimation of Signal Parameters via Rotational Invariance Techniques (ESPRIT) [6], are popularly used to estimate the signal DOAs.

Manuscript received March 4, 2021; revised September 11, 2021; accepted October 18, 2021. Date of publication October 27, 2021; date of current version November 9, 2021. The associate editor coordinating the review of this manuscript and approving it for publication was Dr. Florian Roemer. This work was presented in part at the IEEE Sensor Array and Multichannel Signal Processing Workshop, Hangzhou, China, June 2020 [1], [2]. *(Corresponding author: Yimin D. Zhang.)*

Shuimei Zhang, Ammar Ahmed, and Yimin D. Zhang are with the Department of Electrical and Computer Engineering, Temple University, Philadelphia, PA 19122 USA (e-mail: tug63690@temple.edu; ammar.ahmed@temple.edu; ydzhang@temple.edu).

Shunqiao Sun is with the Department of Electrical and Computer Engineering, The University of Alabama, Tuscaloosa, AL 35487 USA (e-mail: shunqiao.sun@ua.edu).

Digital Object Identifier 10.1109/TSP.2021.3122292

Sparse array designs have attracted significant interests due to its superiority over ULAs in improving the resolution by providing a larger array aperture compared to the ULA counterparts with the same number of sensors [7]–[9]. In the context of difference coarray equivalence, sparse arrays can achieve a higher number of consecutive as well as unique lags, thus significantly increasing the number of degrees-of-freedom (DOFs). A well designed N-sensor sparse array can achieve $\mathcal{O}(N^2)$ DOFs [9]–[16]. A series of signal processing algorithms have been developed to achieve effective DOA estimation using sparse arrays [17]–[25].

Minimum redundancy array (MRA) [7] and minimum hole array (MHA) [9], [26] are two traditional sparse array designs. For a given number of physical sensors, MRA provides the maximum number of consecutive difference lags [7]. MHA, also called Golomb array, provides zero-redundancy difference lags with the minimum number of holes [9], [26]. However, both MRA and MHA do not have general expressions. As a result, they cannot be systematically designed, and their lags and achievable DOFs cannot be easily analyzed. Such shortcomings motivated the development of alternatives sparse array configurations. For example, the nested array [10] consists of two uniform linear subarrays, in which one subarray has a unit interelement spacing. Unlike the MRA and MHA, the sensor positions and the achievable DOFs can be easily determined for a nested array. However, the nested array is sensitive to mutual coupling effects since some of its sensors are closely located. Several variants of the nested array, such as super nested array [13], [14] and augmented nested array [15], are developed to reduce the mutual coupling effect. Another important alternative for mutual coupling reduction is the coprime array. The prototype coprime array [11] consists of a pair of uniform linear subarrays, in which one is of M sensors with an interelement spacing of N units and the other is of N elements with an interelement spacing of M units, where, M and N are a pair of coprime integers. The coprime array was generalized by two operations in [12]. One is the compression of the interelement spacing of one subarray by a positive integer, resulting in a coprime array with compressed interelement spacing (CACIS). The other one is to introduce a displacement between the two subarrrays, resulting in a coprime array with displayed subarrays (CADiS). Compared to the prototype coprime arrays, CACIS and CADiS respectively increase the number of consecutive lags and unique lags. Compared with the nested array, coprime arrays are less sensitive to mutual coupling effects because the

array elements are located with a wider spacing. However, the number of DOFs achieved by coprime arrays is generally lower than that of the nested array counterpart and there are holes in the rendered difference coarray. Some recent efforts have been made to alleviate this problem such as the thinned coprime array [27] and the k-times extended coprime array [28]. The recently developed maximum interelement spacing constraint (MISC) [16] uses three sparse uniform linear subarrays to obtain more DOFs and reduced mutual coupling effects than super nested arrays and augmented nested arrays.

By exploiting the important property that the array manifold is associated with the signal carrier frequency, the concept of constructing a virtual coprime array using a single ULA with two frequencies was developed in [29]. When the two frequencies are associated with a coprime relationship, the signals observed at a single ULA using two frequencies resemble to those observed at a coprime array which consists of two uniform linear subarrays. Accordingly, the coprime array concept is extended to a joint spatio-spectral domain, thereby achieving high flexibility in array structure design to meet both DOF and system complexity constraints. The extension to multiple coprime frequencies, together with the analysis of the achievable number of DOFs, are provided in [30]–[35]. In [33], a method is developed for fast DOA estimation using multi-frequency sparse ULA when the number of sources is less than that of physical sensors. The Cramer-Rao lower bound of the dual-frequency coprime array is analyzed in [34]. Frequency diversity has also been exploited to suppress grating lobes in coherent multi-input multi-output (MIMO) radar with separated subapertures [36]. A wavelength-diverse MIMO radar exploiting multi-frequency signals is considered in [37] where all virtual antenna positions obtained from the MIMO sum coarray and multi-frequency scaling are taken into account. From signal processing perspective, a unique problem to be considered in the DOA estimation using multi-frequency sparse arrays is that, the impinging signals corresponding to different frequencies are not phase synchronized because of unknown phase differences in the target reflection coefficients as well as that in the propagation delays. Therefore, the correlations obtained from self-lag pairs (between signals obtained using the same frequency) and those from cross-lag pairs (between signals obtained using different frequencies) cannot be directly combined [31], [33]. To fuse such self-lag and cross-lag correlation results, existing works on multi-frequency sparse arrays [2], [22], [29], [31] commonly exploit the group-sparsity of these correlation results, i.e., they share a common spatial sparse support corresponding to the signal directions but their values differ.

In [1], we proposed a modified array interpolation method which improves from group sparsity-based methods. The self-lags obtained at each frequency component are incorporated to synthesize the correlation matrix, and a modified structured matrix completion scheme is followed to recover the missing entries in the resulting correlation matrix. As such, the correlation matrix corresponding to the full ULA is recovered, which enables high-resolution and gridless DOA estimation of more sources than the number of self-lags using subspace-based DOA estimation methods. However, such approach only uses the self-lags and, as such, the potential benefits offered by the multi-frequency sparse arrays are not fully exploited. In this paper, we devise a novel approach to enable full utilization of both self- and cross-lags to reconstruct the correlation matrix corresponding to a larger ULA based on structured matrix completion.

Difference coarray-based DOA estimation generally requires a high number of snapshots to enable high-accuracy correlation matrix estimation [38]. In some real-world applications, e.g., automotive radar [39], [40], the requirement of high number of snapshots may not be satisfied because of the rapid variation of the operation environment. In such highly dynamic application scenarios, only a small number of array snapshots are available, particularly when range-Doppler mapping is first considered before performing DOA estimation. In the context of the proposed multi-frequency sparse arrays, on the other hand, the multi-frequency signal observations combined with structured matrix completion offer a high number of DOFs, thereby enabling robust DOA estimation with few data snapshots [1]. It is noted that the proposed method only uses multiple sparse carrier frequencies and, thus, requires a low spectrum occupancy.

To summarize, in this paper, we propose an enhanced DOA estimation framework utilizing generalized multi-frequency sparse arrays. Our contributions are mainly two-fold.

1) We provide flexible multi-frequency sparse array designs to offer a high number of DOFs. Unlike the existing coprime-frequency ULA-based array designs which render high redundancies in the resulting difference lags [29], [31], we exploit nonuniform linear prototype array structures to avoid the lag redundancy issue so that the number of the achieved lags is maximized for the given number of sensors. In the proposed designs, the frequencies do not need to satisfy a coprime relationship, thus providing greater flexibility in the array design.
2) We integrate both self- and cross-lag correlations to synthesize the correlation matrix by exploiting the group sparsity among the signals corresponding to all frequencies, and a modified structured matrix completion scheme exploiting the Hermitian and Toeplitz structures of the correlation matrix reconstructs the full correlation matrix through robust interpolation. As a result, the proposed method allows array designs with a larger aperture compared to [1].

Notations: We use lower-case (upper-case) bold characters to describe vectors (matrices). In particular, $\boldsymbol{I}_L$ stands for the $L \times L$ identity matrix, and $\mathbf{0}_L$ is the $L \times 1$ vector with all zero elements. $(\cdot)^{\mathrm{T}}$ and $(\cdot)^{\mathrm{H}}$ respectively denote the transpose and conjugate transpose of a matrix or vector, and $\mathrm{diag}(\cdot)$ denotes a diagonal matrix with the elements of a vector constituting the diagonal entries. $\|\cdot\|_*$ and $\|\cdot\|_{\mathrm{F}}$ respectively represent the nuclear norm and Frobenius norm. Moreover, $|\cdot|$ denotes the cardinality of a set. $\circ$ is the Hadamard product and $\otimes$ denotes the Kronecker product. In addition, $\mathcal{T}(\boldsymbol{x})$ denotes a Hermitian Toeplitz matrix with $\boldsymbol{x}$ as its first column and $\mathrm{Tr}(\cdot)$ represents the trace operator for a matrix. $\jmath = \sqrt{-1}$ denotes the unit imaginary number. $\mathrm{E}(\cdot)$ denotes the expectation. Finally, $\bigcup$ denotes the union operator.

II. Multi-Frequency Sensor Array

A. Signal Model

Consider a DOA estimation problem in which I continuous-wave signals with carrier frequencies $f_i, i = 1, 2, \ldots, I$, are simultaneously emitted from a single transmit sensor. Extension to multiple transmitter cases is straightforward based on the well-known MIMO radar concept [41]. Assume an L_0-sensor ULA with interelement spacing d, and denote $\mathbb{P} = \{0, 1, 2, \ldots, L_0 - 1\}$. In this paper, we only consider scenarios where M_i takes integer values and satisfies $M_i\lambda_i/2 = d$, where λ_i is the wavelength corresponding to f_i.

The set $\mathbb{S}_i$ containing the sensor positions for the ith frequency, $i = 1, 2, \ldots, I$, is expressed as:

$$\mathbb{S}_i = \{M_i l\bar{d} \,|\, l \in \mathbb{P}\}, \tag{1}$$

where $\bar{d}$ denotes half-wavelength in a normalized frequency sense (i.e., no specific frequency is referred to).

As we discussed earlier, difference coarray reconstruction based on a ULA inherently causes lag redundancies. More specifically, for an L_0-sensor ULA, lag d is repeated by $L_0 - 1$ times, lag $2\,d$ is repeated by $L_0 - 2$ times, and so on. In order to avoid such redundancies and achieve redundancy-free difference coarrays, we consider an L-sensor sparse array design by choosing l from $\mathbb{P}' \subset \mathbb{P}$ with cardinality $|\mathbb{P}'| = L < L_0$ (refer to the design example in Section II-D). In this case, the virtual sensor locations for frequency f_i are given by:

$$\mathbb{S}_i = \{M_i l\bar{d} \,|\, l \in \mathbb{P}'\}. \tag{2}$$

For K uncorrelated far-field targets whose respective DOAs are $\theta_k, k = 1, 2, \ldots, K$, the return signal vector associated with the ith frequency component is expressed as:

$$\tilde{\boldsymbol{x}}_{\mathbb{S}_i}(t) = e^{\jmath 2\pi f_i t} \sum_{k=1}^{K} \rho_k^{(i)}(t)\boldsymbol{a}_{\mathbb{S}_i}(\theta_k) + \tilde{\boldsymbol{n}}_{\mathbb{S}_i}(t), \tag{3}$$

where $\rho_k^{(i)}(t)$ is the reflection coefficient of the kth target for the ith frequency, which is in general frequency-dependent because both target reflectivity and propagation phase delay vary with frequency. In addition,

$$\boldsymbol{a}_{\mathbb{S}_i}(\theta_k) = \left[1, e^{-\jmath\frac{2\pi d_1}{\lambda_i}\sin(\theta_k)}, \ldots, e^{-\jmath\frac{2\pi d_{L-1}}{\lambda_i}\sin(\theta_k)}\right]^{\mathrm{T}} \tag{4}$$

is the steering vector corresponding to θ_k, where d_l is the physical location of the lth element with respect to the reference sensor, and L is the number of physical sensors. The sensor indexed by $l = 0$ is defined as the reference sensor, i.e., $d_0 = 0$. Furthermore, $\tilde{\boldsymbol{n}}_{\mathbb{S}_i}(t) \sim \mathcal{CN}(0, \sigma_n^i \boldsymbol{I}_L)$ denotes the additive white Gaussian noise vector.

After downconverting the received signal vector through separated low-pass filtering corresponding to the respective frequencies, we obtain the following baseband signal model:

$$\begin{aligned}\boldsymbol{x}_{\mathbb{S}_i}(t) &= \sum_{k=1}^{K} \rho_k^{(i)}(t)\boldsymbol{a}_{\mathbb{S}_i}(\theta_k) + \boldsymbol{n}_{\mathbb{S}_i}(t) \\ &= \boldsymbol{A}_{\mathbb{S}_i}\boldsymbol{\rho}^{(i)}(t) + \boldsymbol{n}_{\mathbb{S}_i}(t),\end{aligned} \tag{5}$$

where $\boldsymbol{A}_{\mathbb{S}_i} = [\boldsymbol{a}_{\mathbb{S}_i}(\theta_1), \ldots, \boldsymbol{a}_{\mathbb{S}_i}(\theta_K)]$ and $\boldsymbol{\rho}^{(i)}(t) = [\rho_1^{(i)}(t), \cdots, \rho_K^{(i)}(t)]^{\mathrm{T}}$.

B. Lag Analysis

By incorporating the virtual sensors due to all I frequencies, we define the set $\mathbb{S}$ of the combined sensor positions as:

$$\mathbb{S} = \bigcup_{i=1}^{I} \mathbb{S}_i = \bigcup_{i=1}^{I} \{M_i l\bar{d} \,|\, l \in \mathbb{P}'\}. \tag{6}$$

Note that the reference sensors of all I virtual arrays overlap at the zeroth position. Therefore, the cardinality of $\mathbb{S}$, representing the number of unique virtual sensor positions, is given by

$$|\mathbb{S}| \leq (L-1)I + 1, \tag{7}$$

where the equality is achieved when all virtual sensors do not overlap except at the reference sensor position.

Define the self-lag set as the difference coarray virtual sensor positions obtained from the same frequency, i.e.,

$$\mathbb{C}_{\mathrm{self}} = \bigcup_{i=1}^{I} \mathbb{S}_i \ominus \mathbb{S}_i = \bigcup_{i=1}^{I} \{M_i(l_1 - l_2)\bar{d}\}, \tag{8}$$

where $\ominus$ computes the lags between two sets [42]. Similarly, cross-lags are obtained from all pairs with different frequencies, defined as

$$\mathbb{C}_{\mathrm{cross}} = \bigcup_{\forall i,j,i\neq j} \mathbb{S}_i \ominus \mathbb{S}_j = \bigcup_{\forall i,j,i\neq j} \{(M_i l_1 - M_j l_2)\bar{d}\}, \tag{9}$$

where $l_1, l_2 \in \mathbb{P}'$ and $1 \leq i, j \leq I$. The complete set of the coarray positions constituting all the correlation lags is represented by $\mathbb{C} = \mathbb{C}_{\mathrm{self}} \cup \mathbb{C}_{\mathrm{cross}}$, and the corresponding set of all non-negative correlation lags is denoted as $\mathbb{C}^+$.

While the most important contribution of using multi-frequency signals is to populate the lags significantly beyond that offered by the single-frequency counterparts, it also enables effective mutual coupling mitigation by properly choosing the physical sensor positions and the frequencies that keep a sufficiently large value of $l_1 - l_2$ while synthesizing different lags from $M_i l_1 - M_j l_2$.

C. Analysis of Achievable DOFs

For I mutually coprime frequencies, there are $I(I-1)/2$ co-prime frequency pairs. Given a ULA with L physical sensors, the maximum number of achievable unique lags of the difference coarray generated from different coprime frequency pairs is given by [31]

$$\begin{aligned}\eta &= (L^2-1)(I^2-I) - 2(L-1)(I^2-2I) + 1 \\ &= (L-1)^2 I^2 + (-L^2 + 4\,L - 3)I + 1.\end{aligned} \tag{10}$$

To achieve this upper-bound, a large separation between different frequencies is required to minimize the number of overlapping lags between different frequency pairs.

In this paper, a nonuniform sparse array is utilized such that the lag redundancies are reduced [2]. Following (7), the maximum

TABLE I
COMPARISON BETWEEN THE PREVIOUS AND THE PROPOSED MULTI-FREQUENCY ARRAY DESIGN GIVEN L PHYSICAL SENSORS AND I FREQUENCIES

	Previous multi-frequency array design [31]	Proposed multi-frequency array design
Physical array	Uniform linear array	Nonuniform sparse linear array
Relationship among different frequencies	Coprime	Flexible
Maximum number of unique lags	$(L-1)^2I^2+(-L^2+4L-3)I+1$	$(L-1)^2I^2+(L-1)I+1$

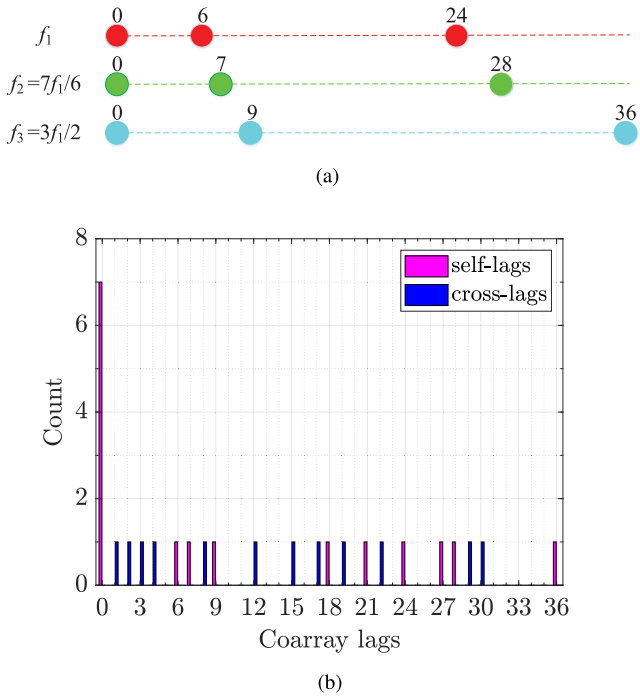

Fig. 1. Illustration of array configuration and histogram of corresponding non-negative difference coarray lags (3 physical sensors and 3 frequencies). (a) Configuration of multi-frequency sparse array. (b) Histogram of corresponding non-negative difference coarray lags.

number of achievable unique lags in the proposed design is given by

$$\eta_{\text{proposed}} = 2\left(\begin{pmatrix}(L-1)I+1\\2\end{pmatrix}\right)+1 = (L-1)^2I^2+(L-1)I+1. \tag{11}$$

It indicates that we can achieve $(\eta_{\text{proposed}}+1)/2$ DOFs. We enlist the comparison between the two array configurations in Table I. The difference in the maximum number of achievable unique lag between [31] and the proposed design is given by

$$\eta_{\text{difference}} = \eta_{\text{proposed}} - \eta = (L-2)(L-1)I. \tag{12}$$

Because $L>2$ is always satisfied, $\eta_{\text{difference}}$ is always positive.

D. Design Example

To have an intuitive understanding, we use a simple example of multi-frequency sparse array configuration with $I=3$ frequencies as illustrated in Fig. 1(a). We set $f_2=7f_1/6$ and $f_3=3f_1/2$. The three frequencies are sparsely separated with a relative bandwidth span of 40%. The sensor positions are chosen for the first frequency as:

$$\mathbb{S}_1 = \{0,6,24\}\lambda_1/2, \tag{13}$$

i.e., $M_1=6$ and $\mathbb{P}'=\{0,1,4\}$. From the frequency ratios, we have $M_2=f_2M_1/f_1=7$ and $M_3=f_3M_1/f_1=9$. Note in this case that M_1 and M_3 are not coprime.

The corresponding sensor locations at the other two frequencies are obtained as:

$$\mathbb{S}_2=\{0,7,28\}\lambda_2/2, \quad \mathbb{S}_3=\{0,9,36\}\lambda_3/2. \tag{14}$$

As a result, the collective sensor positions are given by:

$$\mathbb{S}=\mathbb{S}_1\cup\mathbb{S}_2\cup\mathbb{S}_3=\{0,6,7,9,24,28,36\}\bar{d}. \tag{15}$$

The non-negative self- and cross-lag sets are respectively obtained as:

$$\mathbb{C}^+_{\text{self}}=\{0,6,7,9,18,21,24,27,28,36\}\bar{d}, \tag{16}$$

$$\mathbb{C}^+_{\text{cross}}=\{1,2,3,4,8,12,15,17,19,22,29,30\}\bar{d}. \tag{17}$$

It is noted that the zeroth sensor position is only used to compute the self-lags.

The corresponding non-negative difference coarray positions are obtained as:

$$\begin{aligned}\mathbb{C}^+ &= \mathbb{C}^+_{\text{self}}\bigcup\mathbb{C}^+_{\text{cross}}\\ &= \{0,1,2,3,4,6,7,8,9,12,15,17,18,\\ &\quad 19,21,22,24,27,28,29,30,36\}\bar{d}.\end{aligned} \tag{18}$$

The sensor positions and the difference coarray positions are shown in Fig. 1. This design does not provide a high number of consecutive lags. However, it achieves the highest number of unique lags (i.e., 43 lags) because there are no redundancies in all lags except the unavoidable ones for lag 0.

E. Correlation Matrix

We can estimate the I^2 correlation matrices as:

$$\begin{aligned}\boldsymbol{R}_{\boldsymbol{x}_{\mathbb{S}_i}\boldsymbol{x}_{\mathbb{S}_j}} &= \mathrm{E}\{\boldsymbol{x}_{\mathbb{S}_i}(t)\boldsymbol{x}^{\mathrm{H}}_{\mathbb{S}_j}(t)\}\\ &= \begin{cases}\boldsymbol{A}_{\mathbb{S}_i}\boldsymbol{P}_{i,i}\boldsymbol{A}_{\mathbb{S}_i}+\boldsymbol{\sigma}^2_n\boldsymbol{I}_L, & i=j,\\ \boldsymbol{A}_{\mathbb{S}_i}\boldsymbol{P}_{i,j}\boldsymbol{A}_{\mathbb{S}_j}, & i\neq j,\end{cases}\end{aligned} \tag{19}$$

where $\boldsymbol{P}_{i,i}=\mathrm{E}\{\boldsymbol{\rho}_i(t)\boldsymbol{\rho}^{\mathrm{H}}_i(t)\}$ is a diagonal matrix with positive real values, and $\boldsymbol{P}_{i,j}=\mathrm{E}\{\boldsymbol{\rho}_i(t)\boldsymbol{\rho}^{\mathrm{H}}_j(t)\}$ is a diagonal matrix whose diagonal elements generally take complex values. The phase terms between $\boldsymbol{x}_{\mathbb{S}_i}(t)$ and $\boldsymbol{x}_{\mathbb{S}_j}(t)$, $1\le i,j\le I$, $i\neq j$, depend not only on the spatial angles of the impinging signals but also on the unknown phase difference between the reflection coefficients $\rho^{(i)}_k(t)$ and $\rho^{(j)}_k(t)$ [29].

In practice, the correlation matrix $\boldsymbol{R}_{\boldsymbol{x}_{\mathbb{S}_i}\boldsymbol{x}_{\mathbb{S}_j}}$ is unavailable and is approximated by its sample correlation matrix as:

$$\hat{\boldsymbol{R}}_{\boldsymbol{x}_{\mathbb{S}_i}\boldsymbol{x}_{\mathbb{S}_j}} = \frac{1}{T}\sum_{t=1}^{T} \boldsymbol{x}_{\mathbb{S}_i}(t)\boldsymbol{x}_{\mathbb{S}_j}^{\mathrm{H}}(t), \tag{20}$$

where T is the number of snapshots.

III. DOA Estimation Exploiting Array Interpolation

In this section, we propose a novel DOA estimation algorithm exploiting multi-frequency sparse array interpolation and group sparsity. The concept of array interpolation is employed to generate the same aperture as the L_0-sensor ULA. The resulting correlation matrix enables DOA estimation of much more targets than the number of physical sensors.

A. Array Interpolation With Self-Lags

The received signals of the interpolated ULA can be initialized by augmenting $\boldsymbol{x}_{\mathbb{S}_i}(t)$ as

$$\langle \boldsymbol{y}_{\mathbb{U}}(t)\rangle_{\ell} = \begin{cases} \langle \boldsymbol{x}_{\mathbb{S}_i}(t)\rangle_{\ell}, & \ell\bar{d} \in \mathbb{S}_i, \\ 0, & \ell\bar{d} \in \mathbb{U}\backslash\mathbb{S}_i, \end{cases} \tag{21}$$

where $\mathbb{U} = \mathbb{P}\bar{d}$ and $\langle\cdot\rangle_{\ell}$ denotes the element corresponding to the sensor located at $\ell\bar{d}$. Accordingly, we define an L_0-dimensional binary vector $\boldsymbol{b}_i$ to describe the presence of virtual sensors indexed in the ULA $\mathbb{U}$. Elements of vector $\boldsymbol{b}_i$ with value 1 imply the existence of virtual sensors with frequency f_i, whereas 0 stands for missing virtual sensor positions that have to be interpolated, i.e.,

$$\langle \boldsymbol{b}_i\rangle_{\ell} = \begin{cases} 1, & \ell\bar{d} \in \mathbb{S}_i, \\ 0, & \ell\bar{d} \in \mathbb{U}\backslash\mathbb{S}_i. \end{cases} \tag{22}$$

We initialize the received signals of the interpolated ULA $\boldsymbol{y}_{\mathbb{U}}(t)$ by

$$\boldsymbol{y}_{\mathbb{U}}^{i}(t) = \boldsymbol{x}_{\mathbb{U}}^{i}(t) \circ \boldsymbol{b}_i, \tag{23}$$

where $\boldsymbol{x}_{\mathbb{U}}^{i}(t)$ is the theoretical received signal for frequency f_i using the ULA and is modeled as follows:

$$\boldsymbol{x}_{\mathbb{U}}^{i}(t) = \sum_{k=1}^{K} \rho_k^{(i)}(t)\boldsymbol{a}_{\mathbb{U}}(\theta_k) + \boldsymbol{n}_{\mathbb{U}}^{i}(t) = \boldsymbol{A}_{\mathbb{U}}\boldsymbol{\rho}^{(i)}(t) + \boldsymbol{n}_{\mathbb{U}}^{i}(t), \tag{24}$$

where $\boldsymbol{A}_{\mathbb{U}} = [\boldsymbol{a}_{\mathbb{U}}(\theta_1), \ldots, \boldsymbol{a}_{\mathbb{U}}(\theta_K)]$ and $\boldsymbol{a}_{\mathbb{U}}(\theta_k), k = 1, \ldots, K$ is the array manifold vector of the interpolated ULA corresponding to the kth source and is expressed as:

$$\boldsymbol{a}_{\mathbb{U}}(\theta_k) = \left[1, e^{-\jmath\frac{2\pi d_1}{\lambda_i}\sin(\theta_k)}, \ldots, e^{-\jmath\frac{2\pi d_{L_0-1}}{\lambda_i}\sin(\theta_k)}\right]^{\mathrm{T}}. \tag{25}$$

As we described earlier, unlike coprime array interpolation discussed for the single-frequency arrays in [21], [22], the underlying problem deals with I virtual arrays that share the same L sensors, where the phase terms between $\boldsymbol{x}_{\mathbb{S}_i}(t)$ and $\boldsymbol{x}_{\mathbb{S}_j}(t)$ depend on both the impinging angles and the unknown phase difference between the reflection coefficients. The existence of such unknown phase difference prohibits the direct utilization of the cross-lags obtained from the different frequency pairs, since $\rho_k^{(i)}(t)$ and $\rho_k^{(j)}(t)$ differ in general. Therefore, the array interpolation method developed in [21], [22] cannot be readily applied to the underlying DOA estimation problem.

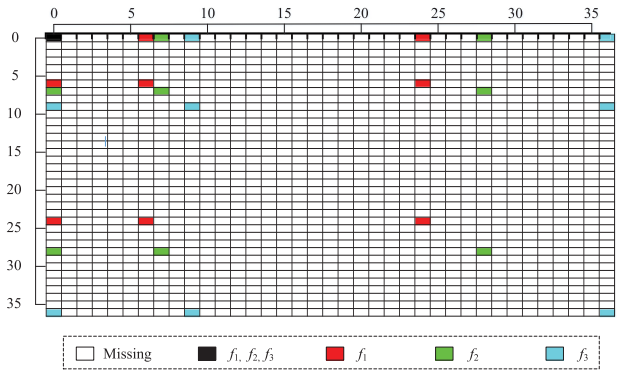

Fig. 2. Binary mask for correlation matrix interpolation using auto-lags.

Based on the fact that the self-lags corresponding to each single-frequency component are not affected by the unknown phase shift, we employ the self-lag set for the array interpolation purpose. To enable effective information fusion of the correlation matrices associated with different frequencies, we define $\boldsymbol{B}_i = \boldsymbol{b}_i\boldsymbol{b}_i^{\mathrm{T}}$ as the mask whose entries distinguish the known and unknown elements in $\hat{\boldsymbol{R}}^{i}_{\boldsymbol{y}_{\mathbb{U}}\boldsymbol{y}_{\mathbb{U}}}$. The synthesized correlation matrix exploiting the I frequencies is given by

$$\hat{\boldsymbol{R}}_{\boldsymbol{y}_{\mathbb{U}}\boldsymbol{y}_{\mathbb{U}}} = \left(\sum_{i=1}^{I} \hat{\boldsymbol{R}}^{i}_{\boldsymbol{x}_{\mathbb{U}}\boldsymbol{x}_{\mathbb{U}}} \circ \boldsymbol{B}_i\right) \circ \boldsymbol{D}, \tag{26}$$

where $\boldsymbol{D}$ is the redundancy averaging matrix. The (m, n)th element in $\boldsymbol{D}$ for $(m, n) \in \{1, \ldots, L_0\}^2$ is obtained by taking the inverse of the overlapping times, expressed as:

$$\boldsymbol{D}(m, n) = \frac{1}{\sum_{i=1}^{I} \boldsymbol{B}_i(m, n) + \epsilon}, \tag{27}$$

where ϵ is a small positive value in order to ensure stability. Accordingly, the $L_0 \times L_0$ binary matrix $\boldsymbol{B}$ distinguishing the observed and missing elements in $\hat{\boldsymbol{R}}_{\boldsymbol{y}_{\mathbb{U}}\boldsymbol{y}_{\mathbb{U}}}$ is

$$\boldsymbol{B} = \boldsymbol{D} \circ \sum_{i=1}^{I} \boldsymbol{B}_i. \tag{28}$$

For the design example illustrated in Fig. 1(a), the positions of the zero entries are represented by the empty boxes depicted in Fig. 2. Red, green and cyan colors respectively denote the entries resulting from frequencies f_1, f_2, and f_3.

As pointed out in [22], conventional matrix completion methods fail to fill in the missing entries in $\hat{\boldsymbol{R}}_{\boldsymbol{y}_{\mathbb{U}}\boldsymbol{y}_{\mathbb{U}}}$ since a number of columns or rows are completely missing. Recalling that, as we consider uncorrelated targets and spatially white noise, the theoretical correlation matrix of a ULA has a Hermitian and Toeplitz structure. Therefore, assuming that the number of targets is smaller than the number of sensors in the interpolated ULA, i.e., $K < L_0$, we can reformulate the correlation matrix recovery problem as the following low-rank structured matrix

completion problem [1]:

$$\begin{aligned} \min_{\boldsymbol{w}} \quad & \operatorname{rank}(\mathcal{T}(\boldsymbol{w})) \\ \text{s.t.} \quad & \left\| \mathcal{T}(\boldsymbol{w}) \circ \boldsymbol{B} - \hat{\boldsymbol{R}}_{\boldsymbol{y}_{\mathbb{U}}\boldsymbol{y}_{\mathbb{U}}} \right\|_{\mathrm{F}}^2 \leq \delta, \\ & \mathcal{T}(\boldsymbol{w}) \succeq 0, \end{aligned} \tag{29}$$

where δ is user-defined parameter, which is related to the noise power. Note that the problem (29) is NP-hard due to the rank minimization [43]. In the following, we relax the rank minimization objective by exploiting the nuclear norm minimization. The nuclear norm of $\mathcal{T}(\boldsymbol{w})$ can be expressed as

$$\|\mathcal{T}(\boldsymbol{w})\|_* = \operatorname{Tr}(\sqrt{\mathcal{T}^{\mathrm{H}}(\boldsymbol{w})\mathcal{T}(\boldsymbol{w})}) = \operatorname{Tr}(\mathcal{T}(\boldsymbol{w})). \tag{30}$$

Then, using the method of Lagrange multipliers [45], we reformulate (29) as the following convex optimization problem [1]:

$$\begin{aligned} \min_{\boldsymbol{w}} \quad & \left\| \mathcal{T}(\boldsymbol{w}) \circ \boldsymbol{B} - \hat{\boldsymbol{R}}_{\boldsymbol{y}_{\mathbb{U}}\boldsymbol{y}_{\mathbb{U}}} \right\|_{\mathrm{F}}^2 + \zeta \operatorname{Tr}(\mathcal{T}(\boldsymbol{w})) \\ \text{s.t.} \quad & \mathcal{T}(\boldsymbol{w}) \succeq 0, \end{aligned} \tag{31}$$

where ζ is a regularization parameter.

The optimization problem in (31) exploits the special properties of the theoretical correlation matrix for the ULA, i.e., Toeplitz and Hermitian, low rank, and positive semidefiniteness. By taking such advantages, we are able to accurately recover the ULA correlation matrix from a small number of virtual sensors and even with a small number of snapshots [1].

B. Array Interpolation Using Both Self- and Cross-Lags

Let $\hat{\mathbf{R}}_{\boldsymbol{y}_{\mathbb{U}}\boldsymbol{y}_{\mathbb{U}}} = \mathbf{U}\boldsymbol{\Sigma}\mathbf{U}^{\mathrm{H}}$ denote its singular value decomposition. Ignoring the noise, the diagonal elements of $\boldsymbol{\Sigma}$ is k-sparse. The coherence of $\mathbf{U}$ is given by [43]

$$\mu(\mathbf{U}) = \frac{L_0}{K} \max_{1 \leq l \leq L_0} \|\mathbf{U}(l,:)\|^2 \in \left[1, \frac{L_0}{K}\right], \tag{32}$$

where $\mathbf{U}(l,:)$ denotes the lth left singular vector of $\hat{\mathbf{R}}_{\boldsymbol{y}_{\mathbb{U}}\boldsymbol{y}_{\mathbb{U}}}$. Matrix $\hat{\boldsymbol{R}}_{\boldsymbol{y}_{\mathbb{U}}\boldsymbol{y}_{\mathbb{U}}}$ has coherence with parameters μ_0 and μ_1 if

1) $\mu(\mathbf{U}) \leq \mu_0$ holds for some positive μ_0;
2) The maximum element of matrix $\sum_{1 \leq k \leq K} \mathbf{u}_k \mathbf{u}_k^{\mathrm{H}}$ is upper bounded by $\mu_1 \sqrt{K}/L_0$ in absolute value for some positive μ_1, where $\mathbf{u}_k$ denotes the kth column of $\mathbf{U}$.

It is shown in [43] that, if the entries of matrix $\hat{\boldsymbol{R}}_{\boldsymbol{y}_{\mathbb{U}}\boldsymbol{y}_{\mathbb{U}}}$ are observed uniformly at random, then there exist constants C and c such that if $|\Omega| \geq C \max(\mu_1^2, \mu_0^{1/2}\mu_1, \mu_0 L_0^{1/4}) \eta K L_0 \log L_0$ holds for some $\eta > 2$, the solution is unique and equal to $\hat{\boldsymbol{R}}_{\boldsymbol{y}_{\mathbb{U}}\boldsymbol{y}_{\mathbb{U}}}$ with probability of $1 - cL_0^{-\eta}$. Therefore, if matrix $\hat{\boldsymbol{R}}_{\boldsymbol{y}_{\mathbb{U}}\boldsymbol{y}_{\mathbb{U}}}$ has a low coherence parameter, it can be completed using a less number of observed entries. For structured matrix completion, the incoherence condition is further relaxed. It is shown that the number of the observed entries in the synthesized correlation matrix must exceed $\mathcal{O}(K \log^4(L_0))$ to guarantee perfect recovery with a high probability under some mild incoherence conditions [44].

From the above analysis, it is clear that more observed entries are required to synthesize a large ULA aperture and detect more targets. The maximum number of non-overlapped entries resulting from the self-correlation matrices $\hat{\boldsymbol{R}}_{\boldsymbol{x}_{\mathbb{S}_i}\boldsymbol{x}_{\mathbb{S}_i}}$ is given by

$$N_{\text{self}} = L^2 I - I + 1, \tag{33}$$

and the maximum number of non-overlapped entries resulting from the cross-correlation matrices $\hat{\boldsymbol{R}}_{\boldsymbol{x}_{\mathbb{S}_i}\boldsymbol{x}_{\mathbb{S}_j}}, i \neq j$, is

$$\begin{aligned} N_{\text{cross}} &= (L^2 - L)I(I-1) - 2(L-1)I \\ &= (L^2 - L)I^2 - (L^2 + L - 2)I. \end{aligned} \tag{34}$$

If we can utilize all the information from all self-lags and cross-lags, the total number of the observed entries becomes:

$$\begin{aligned} N_{\text{total}} &= N_{\text{self}} + N_{\text{cross}} \\ &= (L^2 - L)I^2 - (L-1)I + 1. \end{aligned} \tag{35}$$

The utilization of cross-lags could greatly increase the number of observed entries. For intuitive illustration, the observed entries from the self-lags and cross-lags of the design example in Subsection II-D are shown in Fig. 3(a). By incorporating the Toeplitz property, the equivalent observed entries is depicted in Fig. 3(b). The lag set in Eqs. (16), (17), and (18) are respectively associated to the purple, blue, and their combinations in Fig. 3(b). In Fig. 3(b), we see that the synthesized covariance matrix incorporating the Hermitian Toeplitz property now has entries in

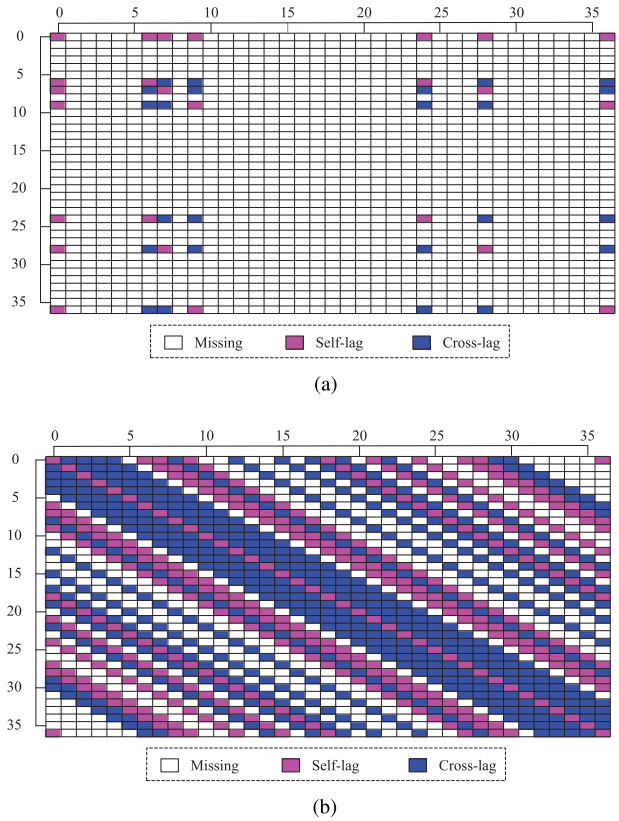

Fig. 3. Observed entries from self-lags and cross-lags in the synthesized correlation matrix. (a) Observed entries in the synthesized correlation matrix. (b) Equivalent observed entries incorporating the Toeplitz structure in the synthesized correlation matrix.

each column and each row, thereby enabling covariance matrix reconstruction in the context of regular matrix completion.

By vectorizing the correlation matrices, we obtain vector $\boldsymbol{z}_{\mathbb{S}_i\mathbb{S}_j} \in \mathcal{C}^{L^2\times 1}$ as [31], [32]:

$$\boldsymbol{z}_{\mathbb{S}_i\mathbb{S}_j} = \mathrm{vec}(\hat{\boldsymbol{R}}_{\boldsymbol{x}_{\mathbb{S}_i}\boldsymbol{x}_{\mathbb{S}_j}}) \approx \begin{cases} \widetilde{\boldsymbol{A}}_{\mathbb{S}_i\mathbb{S}_i}\boldsymbol{p}_{i,i} + \sigma_n^2 \boldsymbol{i}_{\mathbb{S}_i\mathbb{S}_i}, & i = j, \\ \widetilde{\boldsymbol{A}}_{\mathbb{S}_i\mathbb{S}_j}\boldsymbol{p}_{i,j}, & i \neq j, \end{cases} \quad (36)$$

where $\widetilde{\boldsymbol{A}}_{\mathbb{S}_i\mathbb{S}_j} = [\widetilde{\boldsymbol{a}}_{\mathbb{S}_i\mathbb{S}_j}(\theta_1), \ldots, \widetilde{\boldsymbol{a}}_{\mathbb{S}_i\mathbb{S}_j}(\theta_K)]$ with $\widetilde{\boldsymbol{a}}_{\mathbb{S}_i\mathbb{S}_j}(\theta_k) = \boldsymbol{a}^*_{\mathbb{S}_i}(\theta_k) \otimes \boldsymbol{a}_{\mathbb{S}_j}(\theta_k), k = 1, \ldots, K$, and $\boldsymbol{i}_{\mathbb{S}_i\mathbb{S}_i} = \mathrm{vec}(\boldsymbol{I}_L)$. We can reformulate (36) as follows:

$$\boldsymbol{z}_{\mathbb{S}_i\mathbb{S}_j} = \boldsymbol{\Phi}_{\mathbb{S}_i\mathbb{S}_j}\boldsymbol{r}_{i,j},\ i \neq j, \quad (37)$$

where $\boldsymbol{\Phi}_{\mathbb{S}_i\mathbb{S}_j} = [\widetilde{\boldsymbol{a}}_{\mathbb{S}_i\mathbb{S}_j}(\theta_1), \ldots, \widetilde{\boldsymbol{a}}_{\mathbb{S}_i\mathbb{S}_j}(\theta_G), \boldsymbol{0}_{L^2}] \in \mathcal{C}^{L^2\times(G+1)}$ is the dictionary matrix, G is the size of search grid in spatial angles. The positions and values of the non-zero entries in the first G elements of $\boldsymbol{r}_{i,j}$ represent the estimated signal DOAs from cross-lag correlations and the corresponding powers, whereas the last element of $\boldsymbol{r}_{i,j}$ is the estimated noise power.

Given (31), we define

$$\boldsymbol{z}_{\mathbb{U}\mathbb{U}} = \mathrm{vec}(\mathcal{T}(\boldsymbol{w})) = \boldsymbol{\Phi}_{\mathbb{U}\mathbb{U}}\boldsymbol{r} \in \mathcal{C}^{L_0^2\times 1}, \quad (38)$$

where $\boldsymbol{\Phi}_{\mathbb{U}\mathbb{U}} = [\widetilde{\boldsymbol{a}}_{\mathbb{U}\mathbb{U}}(\theta_1), \ldots, \widetilde{\boldsymbol{a}}_{\mathbb{U}\mathbb{U}}(\theta_G), \boldsymbol{i}_{\mathbb{U}\mathbb{U}}]$ is the dictionary matrix corresponding to the interpolated L_0-sensor ULA with $\widetilde{\boldsymbol{a}}_{\mathbb{U}\mathbb{U}}(\theta_g) = \boldsymbol{a}^*_{\mathbb{U}}(\theta_g) \otimes \boldsymbol{a}_{\mathbb{U}}(\theta_g), g = 1, \ldots, G$, $\boldsymbol{i}_{\mathbb{U}\mathbb{U}} = \mathrm{vec}(\boldsymbol{I}_{L_0})$, and $\boldsymbol{r}$ denotes the DOAs estimated from the self-lag correlations. The combined model error accounting for both (37) and (38) is described as

$$\sum_{1\le i<j\le I} \|(\boldsymbol{z}_{\mathbb{S}_i\mathbb{S}_j} - \boldsymbol{\Phi}_{\mathbb{S}_i\mathbb{S}_j}\boldsymbol{r}_{i,j})\|_2 + \|(\boldsymbol{z}_{\mathbb{U}\mathbb{U}} - \boldsymbol{\Phi}_{\mathbb{U}\mathbb{U}}\boldsymbol{r})\|_2. \quad (39)$$

As indicated in [2], [31], [34], the received signal vectors corresponding to different frequencies share a common spatial support representing the same signal DOAs, but generally have distinct coefficients. Therefore, we can view the DOA estimation problem as a group-sparse reconstruction problem to incorporate the cross-lags in the array interpolation procedure.

Based on the above discussion, the array interpolation problem in (31) is modified to further account for the constraint described in (39) using the method of Lagrange multipliers and to utilize the group-sparsity in the spatial support among different frequencies, yielding the following optimization problem:

$$\begin{aligned} \min_{\boldsymbol{w},\boldsymbol{\mathcal{R}}} \quad & \left\|\mathcal{T}(\boldsymbol{w}) \circ \boldsymbol{B} - \hat{\boldsymbol{R}}_{\boldsymbol{y}_{\mathbb{U}}\boldsymbol{y}_{\mathbb{U}}}\right\|_{\mathrm{F}}^2 + \zeta\,\mathrm{Tr}\,(\mathcal{T}(\boldsymbol{w})) \\ & + \beta_1 \sum_{1\le i<j\le I} \|(\boldsymbol{z}_{\mathbb{S}_i\mathbb{S}_j} - \boldsymbol{\Phi}_{\mathbb{S}_i\mathbb{S}_j}\boldsymbol{r}_{i,j})\|_2 \\ & + \beta_1 \|(\boldsymbol{z}_{\mathbb{U}\mathbb{U}} - \boldsymbol{\Phi}_{\mathbb{U}\mathbb{U}}\boldsymbol{r})\|_2 + \beta_2 \|\boldsymbol{\mathcal{R}}\|_{1,2} \\ \text{s.t.} \quad & \mathcal{T}(\boldsymbol{w}) \succeq 0, \end{aligned} \quad (40)$$

where $\boldsymbol{\mathcal{R}} = [\boldsymbol{r}_{1,2}, \boldsymbol{r}_{1,3}, \ldots, \boldsymbol{r}_{I-1,I}, \boldsymbol{r}] \in \mathcal{C}^{(G+1)\times(I(I-1)/2+1)}$ and its mixed $\ell_{1,2}$-norm is defined as

$$\|\boldsymbol{\mathcal{R}}\|_{1,2} = \sum_{m=1}^{G+1} \left(\sum_{n=1}^{I(I-1)/2+1} \mathcal{R}(m,n)\mathcal{R}^*(m,n) \right)^{1/2}, \quad (41)$$

with $\mathcal{R}(m,n)$ denoting the element of $\boldsymbol{\mathcal{R}}$ located at the mth row and the nth column. In addition, β_1 and β_2 are regularization parameters which respectively control the data-fitting error and the group-sparsity term. We see that the proposed method degenerates to (31) [1] when $\beta_1 = \beta_2 = 0$. In general, a higher value of β_1 will put more weights to the cross-lags in determining the solutions, and high values of ζ and β_2 would yield more sparse DOA estimates. It is noted that the on-grid assumption is required in (40) due to the incorporation of the cross-lag correlations. The problem (40) is convex [45] and can be solved using, e.g., CVX [46]. We obtain the estimated synthesis matrix $\mathcal{T}(\hat{\boldsymbol{w}})$ and $\hat{\boldsymbol{\mathcal{R}}}$. $\mathcal{T}(\hat{\boldsymbol{w}})$ is selected for further DOA estimation. On one hand, $\mathcal{T}(\hat{\boldsymbol{w}})$ is strictly Toeplitz, which can help to obtain a better performance. On the other hand, it is easier to specify the number of the targets and avoid spurious peaks if we apply the subspace-based DOA estimation method on $\mathcal{T}(\hat{\boldsymbol{w}})$ instead of obtaining the DOA directly from $\hat{\boldsymbol{\mathcal{R}}}$. In this paper, we exploit the MUSIC algorithm [5] to perform the DOA estimation, given its good angular resolution and computational complexity.

IV. Simulation Results

In this section, we present simulation results to demonstrate the DOA estimation performance of the proposed method. The design example in Section II-D is considered which exploits $I = 3$ frequencies and $L = 3$ physical sensors. It corresponds to $|\mathbb{S}| = 7$ virtual sensors from the three frequencies and $|\mathbb{P}| = L_0 = 37$ sensors in the interpolated ULA. The regularization parameters ζ, β_1, and β_2 for correlation matrix recovery are set to 0.5, 1, and 0.5, respectively. The noise power at the three frequencies are assumed to be the same. Unless otherwise specified, the input SNR values for all sources are assumed to be identical. The phase difference between the received signal corresponding to different frequencies is independently and uniformly distributed in $[0, 2\pi)$. The grid interval is set to 0.1°. We compare the proposed method with the structural matrix completion method exploiting the self-lags [1] and the group sparsity-based method using both self- and cross-lags without array interpolation [2], [31]. Group lasso [47] is employed to solve all group sparse reconstruction problems.

It is noted that the MUSIC pseudo-spectra are presented in dB whereas the spectra obtained from the group lasso are presented in the linear scale.

A. Example 1: $K = 4$ Nonuniform Distributed Targets

We first consider $K = 4$ targets that are nonuniformly located at $[-19^\circ, -15^\circ, 5^\circ, 9^\circ]$. Note that the number of targets exceeds the number of physical sensors. The input SNR is 10 dB for all targets and the number of snapshots is set to 50. We observe in Fig. 4(a) that the group lasso-based method without array interpolation detects the 4 targets but spurious peaks appear in the estimated spatial spectrum. Such distorted spatial spectrum is due to the inaccurate covariance matrix estimation from a small number of snapshots. On the other hand, the two array interpolation methods, respectively presented in Fig. 4(b) using self-lag correlations and in Fig. 4(c) for the the proposed method

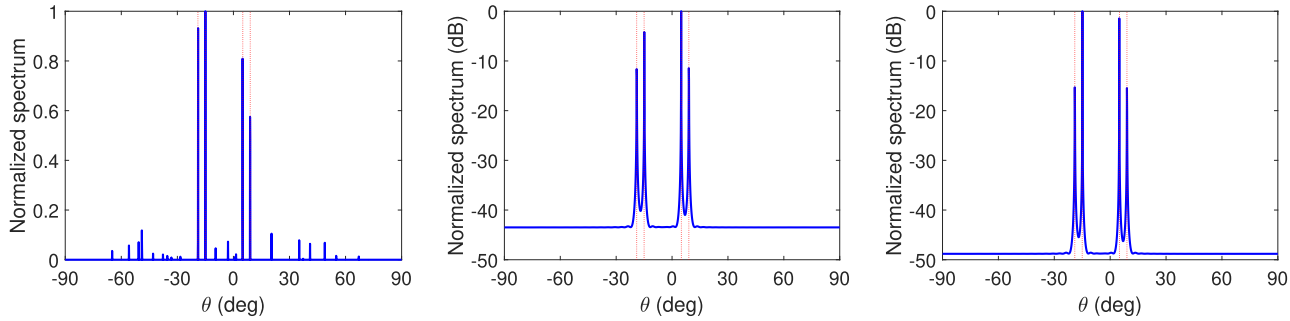

(a) (b) (c)

Fig. 4. Comparison of DOA estimation results. $K = 4$ targets located at $[-19°, -15°, 5°, 9°]$. Input SNR $= 10$ dB for all targets, and $T = 50$. (a) Group lasso without array interpolation [2]. (b) Array interpolation with self-lags [1]. (c) Proposed array using both self- and cross-lags.

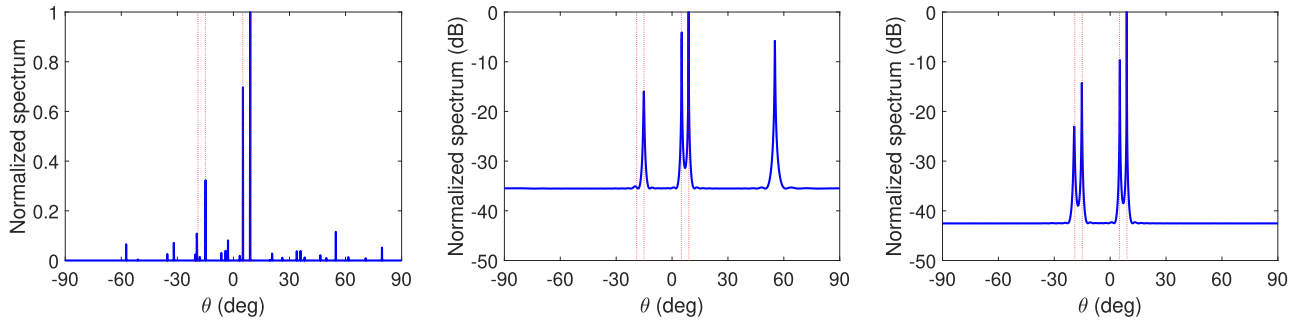

(a) (b) (c)

Fig. 5. Comparison of DOA estimation results. $K = 4$ targets, located at $[-19°, -15°, 5°, 9°]$, have respective input SNR of 5, 10, 12, and 15 dB. $T = 50$. (a) Group lasso without array interpolation [2]. (b) Array interpolation with self-lags [1]. (c) Proposed array using both self- and cross-lags.

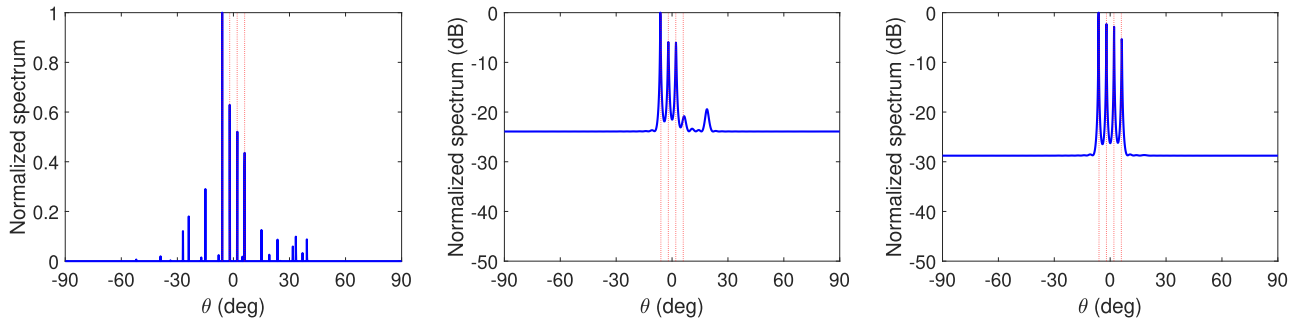

(a) (b) (c)

Fig. 6. Comparison of DOA estimation results. $K = 4$ targets are uniformly distributed in $[-6°, 6°]$. Input SNR $= 10$ dB for all targets, and $T = 50$. (a) Group lasso without array interpolation [2]. (b) Array interpolation with self-lags [1]. (c) Proposed array using both self- and cross-lags.

using both self- and cross-lags, resolve the 4 targets accurately. The proposed method depicted in Fig. 4(c) provides a lower spectrum floor compared to the results presented in Fig. 4(b).

B. Example 2: $K = 4$ Nonuniform Distributed Targets With Unequal Strength

In this example, we consider the same four targets as considered in Section IV-A but they assume different input SNR values of 5, 10, 12, and 15 dB. The group lasso-based method is sensitive to the amplitude difference among targets. As depicted in Fig. 5(a), the highest 4 peaks are no longer correctly associated with the 4 targets, as the target at $-19°$ yields a lower amplitude than the spurious peak at $54.8°$. For the array interpolation method using only self-lags in Fig. 5(b), the target at $-19°$ appears as a biased and very low peak whereas a spurious peak appears at $55.2°$. Fig. 5(c) presents the result of the proposed method. The four targets are detected at $[-19.3°, -15.2°, 5.2°, 9°]$, respectively. We see that the unequal SNR levels result in degraded DOA estimation performance for the weak targets, and the proposed method provides enhanced robustness.

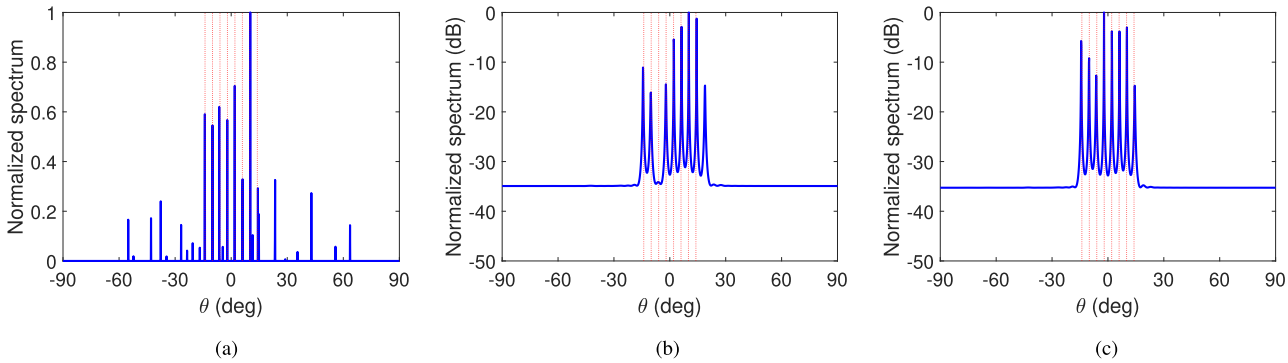

(a) (b) (c)

Fig. 7. Comparison of DOA estimation results. $K = 8$ targets are uniformly distributed in $[-14°, 14°]$. Input SNR $= 10$ dB for all targets, and $T = 100$. (a) Group lasso without array interpolation [2]. (b) Array interpolation with self-lags [1]. (c) Proposed array using both self- and cross-lags.

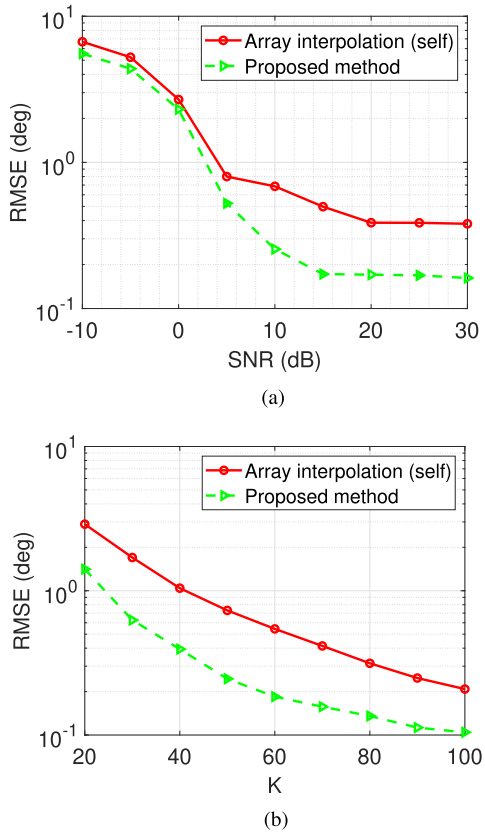

(a) (b)

Fig. 8. RMSE versus the input SNR and the number of snapshots. (a) RMSE versus input SNR ($K = 50$ snapshots). (b) RMSE versus number of snapshots (SNR $= 10$ dB).

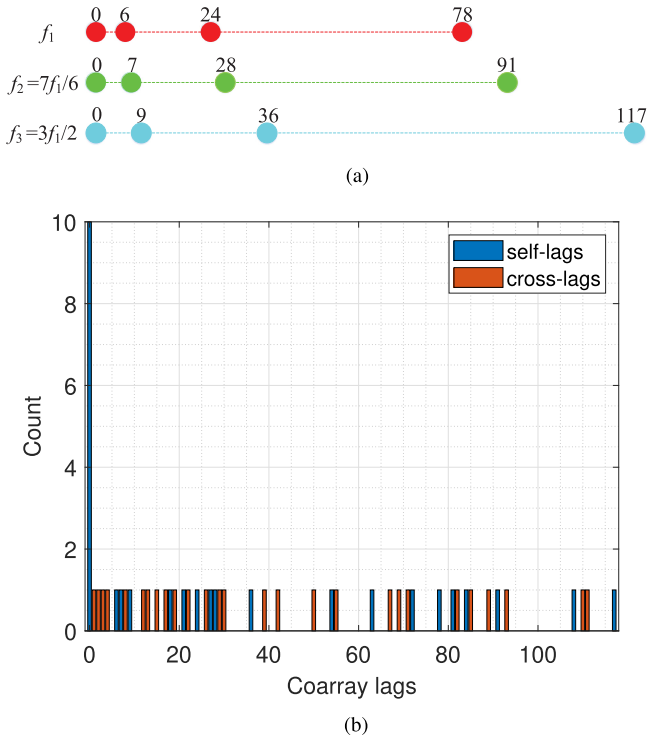

(a) (b)

Fig. 9. Illustration of array configuration and histogram of corresponding non-negative difference coarray lags (4 physical sensors and 3 frequencies). (a) Configuration of multi-frequency sparse array. (b) Histogram of corresponding non-negative difference coarray lags.

C. *Example 3:* $K = 4$ *Closely Distributed Targets*

In this example, we change the four targets in Section IV-A to angles $[-6°, -2°, 2°, 6°]$, which are uniformly but more closely distributed. The closer angle separations degrade the group lasso-based method with more spurious peaks as depicted in Fig. 6(a). From Fig. 6(b), for the array interpolation method using only self-lag correlations, there exists a spurious peak in $18.9°$ whose level is higher that the spectrum located in $6°$. Fig. 6(c) presents the estimated spectrum of proposed method which incorporates both self- and cross-lag correlations, where all four targets are correctly detected without spurious peaks.

D. *Example 4:* $K = 8$ *Closely Distributed Targets*

In this example, we consider a higher number of $K = 8$ targets which are uniformly distributed between $-14°$ and $-14°$. The input SNR for all targets is 10 dB, and 100 snapshots are used. Note in this case that the number of targets exceeds the number of virtual sensors ($|\mathbb{S}| = 7$) resulting from the three frequencies. Fig. 7(a) presents the spatial spectrum obtained by the group lasso-based method. While the highest peaks indicate

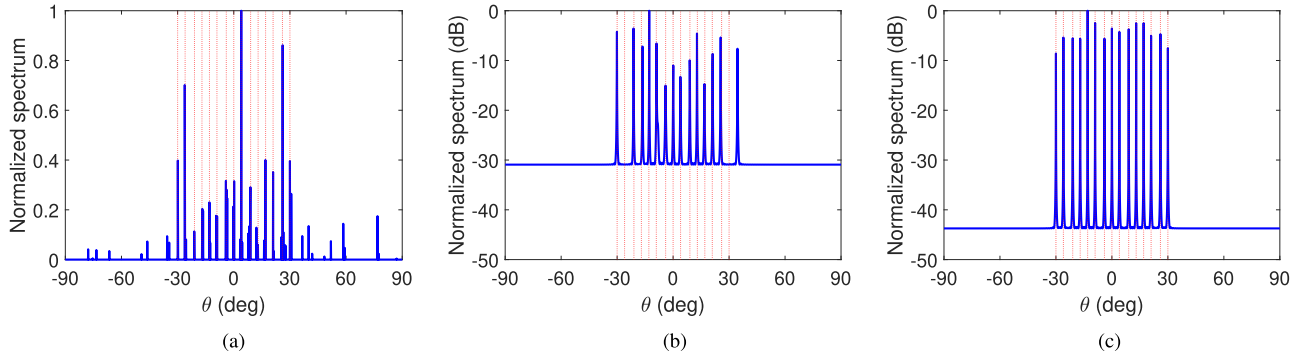

Fig. 10. Comparison of DOA estimation results for the array depicted in Fig. 9. $K = 15$ targets are uniformly distributed in $[-30^\circ, 30^\circ]$. Input SNR $= 10$ dB and $T = 200$. (a) Group-lasso with self- and cross-lags [2]. (b) Array interpolation with self-lags [1]. (c) Proposed array using both self- and cross-lags.

the targets, a high number of spurious peaks appear with a moderate magnitude. For the array interpolation exploiting only self-lags, as depicted in Fig. 7(b), one target is missing and one high spurious peak appears in 18.8°. By utilizing both self- and cross-lags in the synthesis of the correlation matrix, the proposed method provides accurate DOA estimation of all targets with no spurious peaks, as depicted in Fig. 7(c).

E. Robustness Analysis

In this subsection, we quantitatively compare the performance of the proposed DOA estimation strategy in terms of root mean squared error (RMSE) with respect to the input SNR and the number of snapshots. The RMSE is defined as:

$$\text{RMSE} = \sqrt{\frac{1}{NK}\sum_{n=1}^{N}\sum_{k=1}^{K}\left(\hat{\theta}_{k,n} - \theta_k\right)^2}, \tag{42}$$

where $\hat{\theta}_{k,n}$ denotes the estimate of the kth target direction θ_k in the nth Monte-Carlo trial. 500 independent trials are utilized to generate each result. The case described in Section IV-C, i.e., 4 targets uniformly distributed in $[-6^\circ, 6^\circ]$, is selected for RMSE comparison. It is noted that the group lasso-based method is excluded for RMSE comparison due to the presence of excessive amount of spurious peaks in its results.

Fig. 8(a) shows the RMSE performance with respect to the input SNR, where 50 snapshots are used. It is observed that the proposed method consistently outperforms the array interpolation method utilizing only the self-lags, particularly when the SNR is 10 dB and higher. Fig. 8(b) depicts the RMSE performance with respect to the number of snapshots. It is observed again that the proposed method consistently achieves a much lower RMSE than the array interpolation method using self-lag correlations.

F. Generalization Analysis

In this subsection, we consider another zero-redundancy sparse array design which consists of 4 physical sensors and 3 frequencies. The sparse array and the corresponding lags are illustrated in Fig. 9.

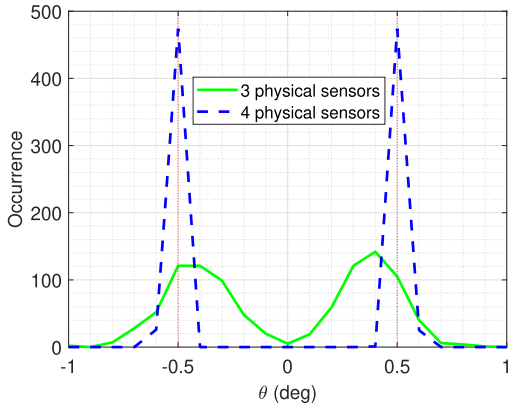

Fig. 11. Histogram of DOA estimates exploiting MUSIC obtained from 500 Monte Carlo trials for the proposed method. $K = 2$ targets are located at $[-0.5^\circ, 0.5^\circ]$. Input SNR $= 10$ dB for both targets and $T = 20$.

Consider that $K = 15$ targets are uniformly spaced between -30° and 30°. The input SNR is 10 dB for all targets and 200 snapshots are adopted. The DOA estimation results are presented in Fig. 10. For the group lasso-based results depicted in Fig. 10(a), we observe that a high number of spurious peaks obscure the spatial spectrum. For the array interpolation method using self-lags only, Fig. 10(b) shows that two targets are not correctly detected. In comparison, the proposed method successfully resolves all 15 targets. Next, we compare the capability of the two proposed array designs, namely the 3-element array depicted in Fig. 1(a) and the 4-element array depicted in Fig. 9(a), in resolving closely spaced targets. We consider two closely spaced targets respectively located at $[-0.5^\circ, 0.5^\circ]$, and the input SNR for both targets is 10 dB. The number of snapshots is reduced to 20. The histogram of 500 Monte Carlo trials shown in Fig. 11 reveals that the result of the 4-element array gives more accurate DOA estimation than that offered by the 3-element array counterpart.

V. Conclusion

In this paper, we proposed a multi-frequency sparse array framework that can provide high-resolution DOA estimation

capability and resolve much more targets than the number of physical sensors. Both self- and cross-lags are utilized for array interpolation. Therefore, the achievable DOFs have been greatly enhanced. In particular, we incorporate the cross-lags into the synthesized correlation matrix by exploiting the group-sparsity among different frequencies. Simulation results demonstrated that the proposed strategy provides promising performance for the DOA estimation.

REFERENCES

[1] S. Zhang, A. Ahmed, Y. D. Zhang, and S. Sun, "DOA estimation exploiting interpolated multi-frequency sparse array," in *Proc. IEEE Sensor Array Multichannel Signal Process. Workshop*, Hangzhou, China, 2020, pp. 1–5.

[2] A. Ahmed, D. Silage, and Y. D. Zhang, "High-resolution target sensing using multi-frequency sparse array," in *Proc. IEEE Sensor Array Multichannel Signal Process. Workshop*, Hangzhou, China, 2020, pp. 1–5.

[3] H. L. Van Trees, *Detection, Estimation, and Modulation Theory, Part IV: Optimum Array Processing*. New York, NY, USA: Wiley, 2002.

[4] T. E. Tuncer and B. Friedlander Eds., *Classical and Modern Direction-of-Arrival Estimation*. Burlington, MA, USA: Elsevier, 2009.

[5] R. O. Schmidt, "Multiple emitter location and signal parameter estimation," *IEEE Trans. Antennas Propag.*, vol. AP-34, no. 3, pp. 276–280, Mar. 1986.

[6] R. Roy and T. Kailath, "ESPRIT-estimation of signal parameters via rotational invariance techniques," *IEEE Trans. Acoust., Speech, Signal Process.*, vol. 37, no. 7, pp. 984–995, Jul. 1989.

[7] A. Moffet, "Minimum-redundancy linear arrays," *IEEE Trans. Antennas Propag.*, vol. AP-16, no. 2, pp. 172–175, Mar. 1968.

[8] R. T. Hoctor and S. A. Kassam, "The unifying role of the co-array in aperture synthesis for coherent and incoherent imaging," *Proc. IEEE*, vol. 78, no. 4, pp. 735–752, Apr. 1990.

[9] A. Ahmed and Y. D. Zhang, "Generalized non-redundant sparse array designs," *IEEE Trans. Signal Process.*, vol. 69, pp. 4580–4594, Aug. 2021.

[10] P. Pal and P. P. Vaidyanathan, "Nested arrays: A novel approach to array processing with enhanced degrees of freedom," *IEEE Trans. Signal Process.*, vol. 58, no. 8, pp. 4167–4181, Aug. 2010.

[11] P. P. Vaidyanathan and P. Pal, "Sparse sensing with co-prime samplers and arrays," *IEEE Trans. Signal Process.*, vol. 59, no. 2, pp. 573–586, Feb. 2011.

[12] S. Qin, Y. D. Zhang, and M. G. Amin, "Generalized coprime array configurations for direction-of-arrival estimation," *IEEE Trans. Signal Process.*, vol. 63, no. 6, pp. 1377–1390, Mar. 2015.

[13] C.-L. Liu and P. P. Vaidyanathan, "Super nested arrays: Linear sparse arrays with reduced mutual coupling—Part I: Fundamentals," *IEEE Trans. Signal Process.*, vol. 64, no. 15, pp. 3997–4012, Aug. 2016.

[14] C.-L. Liu and P. P. Vaidyanathan, "Super nested arrays: Linear sparse arrays with reduced mutual coupling—Part II: High-order extensions," *IEEE Trans. Signal Process.*, vol. 64, no. 16, pp. 4203–4217, Aug. 2016.

[15] J. Liu, Y. Zhang, Y. Lu, S. Ren, and S. Cao, "Augmented nested arrays with enhanced DOF and reduced mutual coupling," *IEEE Trans. Signal Process.*, vol. 65, no. 21, pp. 5549–5563, Nov. 2017.

[16] Z. Zheng, W.-Q. Wang, Y. Kong, and Y. D. Zhang, "MISC array: A new sparse array design achieving increased degrees of freedom and reduced mutual coupling effect," *IEEE Trans. Signal Process.*, vol. 67, no. 7, pp. 1728–1741, Apr. 2019.

[17] Y. D. Zhang, M. G. Amin, and B. Himed, "Sparsity-based DOA estimation using co-prime arrays," in *Proc. IEEE Int. Conf. Acoust., Speech, Signal Process.*, Vancouver, Canada, 2013, pp. 3967–3971.

[18] Q. Shen, W. Liu, W. Cui, S. Wu, Y. D. Zhang, and M. G. Amin, "Low-complexity direction-of-arrival estimation based on wideband co-prime arrays," *IEEE/ACM Trans. Audio, Speech Lang. Process.*, vol. 23, no. 9, pp. 1445–1456, Sep. 2015.

[19] S. Qin, Y. D. Zhang, and M. G. Amin, "DOA estimation of mixed coherent and uncorrelated targets exploiting coprime MIMO radar," *Digit. Signal Process.*, vol. 61, pp. 26–34, Feb. 2017.

[20] C. Zhou, Y. Gu, Y. D. Zhang, Z. Shi, T. Jin, and X. Wu, "Compressive sensing based coprime array direction-of-arrival estimation," *IET Commun.*, vol. 11, no. 11, pp. 1719–1724, Aug. 2017.

[21] C. Zhou, Y. Gu, X. Fan, Z. Shi, G. Mao, and Y. D. Zhang, "Direction-of-arrival estimation for coprime array via virtual array interpolation," *IEEE Trans. Signal Process.*, vol. 66, no. 22, pp. 5956–5971, Nov. 2018.

[22] C. Zhou, Y. Gu, Z. Shi, and Y. D. Zhang, "Off-grid direction-of-arrival estimation using coprime array interpolation," *IEEE Signal Process. Lett.*, vol. 25, no. 11, pp. 1710–1714, Nov. 2018.

[23] P. Gupta and M. Agrawal, "Design and analysis of the sparse array for DoA estimation of noncircular signals," *IEEE Trans. Signal Process.*, vol. 67, no. 2, pp. 460–473, Jan. 2019.

[24] Z. Zheng, M. Fu, W. Wang, S. Zhang, and Y. Liao, "Localization of mixed near-field and far-field sources using symmetric double-nested arrays," *IEEE Trans. Antennas Propag.*, vol. 67, no. 11, pp. 7059–7070, Nov. 2019.

[25] Z. Li, X. Zhang, P. Gong, and C. Wang, "Sparse nested linear array for direction of arrival estimation," *Signal Process.*, vol. 169, Apr. 2020, Art. no. 107372.

[26] G. S. Bloom and S. W. Golomb, "Application of numbered undirected graphs," *Proc. IEEE*, vol. 65, no. 4, pp. 562–570, Apr. 1977.

[27] A. Raza, W. Liu, and Q. Shen, "Thinned coprime array for second-order difference co-array generation with reduced mutual coupling," *IEEE Trans. Signal Process.*, vol. 67, no. 8, pp. 2052–2065, Apr. 2019.

[28] X. Wang and X. Wang, "Hole identification and filling in k-times extended co-prime arrays for highly-efficient DOA estimation," *IEEE Trans. Signal Process.*, vol. 67, no. 10, pp. 2693–2706, May 2019.

[29] Y. D. Zhang, M. G. Amin, F. Ahmad, and B. Himed, "DOA estimation using a sparse uniform linear array with two CW signals of co-prime frequencies," in *Proc. 5th IEEE Int. Workshop Comput. Adv. Multi-Sensor Adaptive Process.*, Saint Martin, 2013, pp. 404–407.

[30] S. Qin, Y. D. Zhang, and M. G. Amin, "DOA estimation exploiting coprime frequencies," in *Proc. SPIE*, vol. 9103, no. 91030E, Baltimore, MD, May 2014, pp. 1–7.

[31] S. Qin, Y. D. Zhang, M. G. Amin, and B. Himed, "DOA estimation exploiting a uniform linear array with multiple co-prime frequencies," *Signal Process.*, vol. 130, pp. 37–46, Jan. 2017.

[32] A. Ahmed, Y. D. Zhang, and B. Himed, "Cumulant-based direction-of-arrival estimation using multiple co-prime frequencies," in *Proc. Asilomar Conf. Signals, Syst., Comput.*, Pacific Grove, CA, USA, 2017, pp. 1188–1192.

[33] A. Liu, X. Zhang, Q. Yang, and W. Deng, "Fast DOA estimation algorithms for sparse uniform linear array with multiple integer frequencies," *IEEE Access*, vol. 6, pp. 29952–29965, May 2018.

[34] M. Guo, Y. D. Zhang, and T. Chen, "Performance analysis for uniform linear arrays exploiting two coprime frequencies," *IEEE Signal Process. Lett.*, vol. 25, no. 6, pp. 838–842, Jun. 2018.

[35] M. Guo, Y. D. Zhang, and T. Chen, "Compressive measurements exploiting coprime frequencies for direction finding," in *Proc. IEEE Sensor Array Multichannel Signal Process. Workshop*, Sheffield, U.K., 2018, pp. 26–30.

[36] L. Zhuang and X. Liu, "Application of frequency diversity to suppress grating lobes in coherent MIMO radar with separated subapertures," *EURASIP J. Adv. Signal Process.*, vol. 2009, pp. 1–10, 2009.

[37] M. Ulrich and B. Yang, "Wavelength-diverse MIMO radar: Parameter-coupling, array-carrier optimization and direction-of-arrival estimation," *IEEE Trans. Aerosp. Electron. Syst.*, vol. 55, no. 4, pp. 1920–1932, Aug. 2019.

[38] Y. Liu and J. R. Buck, "High-resolution direction-of-arrival estimation in SNR and snapshot challenged scenarios using multi-frequency coprime arrays," in *Proc. IEEE Int. Conf. Acoust., Speech, Signal Process.*, New Orleans, LA, 2017, pp. 3434–3438.

[39] S. Sun, A. P. Petropulu, and H. V. Poor, "MIMO radar for advanced driver-assistance systems and autonomous driving: Advantages and challenges," *IEEE Signal Process. Mag.*, vol. 37, no. 4, pp. 98–117, Jul. 2020.

[40] S. Sun and Y. D. Zhang, "4D automotive radar sensing for autonomous vehicles: A sparsity-oriented approach," *IEEE Sel. Topics Signal Process.*, vol. 15, no. 4, pp. 879–891, Jun. 2021.

[41] J. Li and P. Stoica, *MIMO Radar Signal Processing*. Hoboken, NJ, USA: Wiley, 2008.

[42] A. Ahmed, Y. D. Zhang, and J.-K. Zhang, "Coprime array design with minimum lag redundancy," in *Proc. IEEE Int. Conf. Acoust., Speech, Signal Process.*, Brighton, U.K., 2019, pp. 4125–4129.

[43] E. J. Candès and B. Recht, "Exact matrix completion via convexoptimization," *Found. Comput. Math.*, vol. 9, no. 6, pp. 717–772, 2009.

[44] Y. Chen and Y. Chi, "Robust spectral compressed sensing via structured matrix completion," *IEEE Trans. Inf. Theory*, vol. 60, no. 10, pp. 6576–6601, Oct. 2014.

[45] S. Boyd and L. Vandenberghe, *Convex Optimization*. Cambridge, U.K.: Cambridge Univ. Press, 2004.

[46] M. Grant, S. Boyd, and Y. Ye, "CVX: MATLAB software for disciplined convex programming, Version 2.2," Jan. 2020. Accessed: Oct. 31, 2021. [Online]. Available: http://cvxr.com/cvx/.

[47] L. Meier, S. V. D. Geer, and P. Bühlmann, "The group lasso for logistic regression," *J. Roy. Statist. Soc. B*, vol. 70, no. 1, pp. 53–71, Feb. 2008.

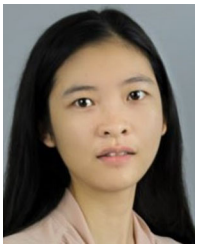

Shuimei Zhang (Member, IEEE) received the B.S. and M.S. degrees in engineering from Hunan University, Changsha, China, in 2013 and 2016, respectively, and the Ph.D. degree in electrical engineering from Temple University, Philadelphia, PA, USA, in 2021. She is currently a Radar Signal Processing Engineer with Aptiv, Agoura Hills, CA, USA. Her research interests include automotive radar, time-frequency analysis, array signal processing, compressive sensing, and machine learning.

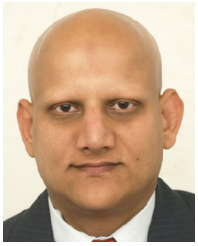

Ammar Ahmed (Student Member, IEEE) received the Ph.D. degree in electrical engineering from Temple University, Philadelphia, PA, USA, in 2021. He is currently a Radar Signal Processing Engineer with Aptiv, Agoura Hills, CA, USA. His research interests include digital signal processing, optimization, and radar systems.

Yimin D. Zhang (Fellow, IEEE) received the Ph.D. degree from the University of Tsukuba, Tsukuba, Japan, in 1988.

He is currently an Associate Professor with the Department of Electrical and Computer Engineering, Temple University, Philadelphia, PA, USA. From 1998 to 2015, he was a Research Faculty with the Center for Advanced Communications, Villanova University, Villanova, PA, USA. His research interests include array signal processing, compressive sensing, machine learning, convex optimization, and time-frequency analysis with applications to radar, wireless communications, and satellite navigation.

Dr. Zhang is an Associate Editor for the IEEE TRANSACTIONS ON AEROSPACE AND ELECTRONIC SYSTEMS and *Signal Processing*. He was an Associate Editor for the IEEE TRANSACTIONS ON SIGNAL PROCESSING, IEEE SIGNAL PROCESSING LETTERS, and *Journal of the Franklin Institute*. He is a Member of the Signal Processing Theory and Methods Technical Committee of the IEEE Signal Processing Society. He was a Technical Co-Chair of the 2018 IEEE Sensor Array and Multichannel Signal Processing Workshop. He was a recipient of the 2016 IET Radar, Sonar & Navigation Premium Award, the 2017 IEEE AESS Harry Rowe Mimno Award, the 2019 IET Communications Premium Award, and the 2021 EURASIP Best Paper Award for Signal Processing. He coauthored a paper that received the 2018 IEEE Signal Processing Society Young Author Best Paper Award. He is a Fellow of SPIE.

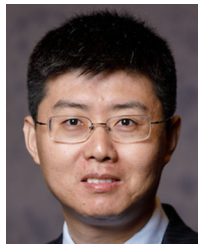

Shunqiao Sun (Senior Member, IEEE) received the Ph.D. degree in electrical and computer engineering from Rutgers, The State University of New Jersey, New Brunswick, NJ, USA, in Janurary 2016. In August 2019, he joined the Department of Electrical and Computer Engineering, The University of Alabama, Tuscaloosa, AL, USA, as a tenure-track Assistant Professor. From 2016 to 2019, he was with the Radar Core Team of Aptiv, Technical Center Malibu, CA, USA, where he has worked on advanced radar signal processing and machine learning algorithms for self-driving cars. In the past, he held internships with Mitsubishi Electric Research Labs, Cambridge, MA, USA, and Cisco Systems, Shanghai, China. His research interests include the interface of statistical and sparse signal processing with mathematical optimizations, MIMO radar, automotive radar, remote sensing, machine learning, connected and autonomous vehicles. Dr. Sun has been awarded the 2015-2016 Rutgers University ECE Graduate Program Academic Achievement Award. He is also the winner of 2016 IEEE Aerospace and Electronic Systems Society Robert T. Hill Best Dissertation Award for his thesis MIMO Radar with Sparse Sensing.